Implementation and Evaluation of a 10 Gbps Real-time FSO Link

Zun Htay[1], Nithin Mohan[1], Mojtaba Mansour Abadi[1], Zabih Ghassemlooy[1], Andrew Burton[2], Stanislav Zvanovec[3]

[1] Optical Communications Research Group, Faculty of Engineering and Environment, Northumbria University, Newcastle upon Tyne, NE1 8ST, UK
[2] Isocom Limited, 2 Fern Court, Bracken Hill Business Park, Peterlee, SR8 2RR, UK
[3] Department of Electromagnetic Field, Faculty of Electrical Engineering, Czech Technical University in Prague, Prague 16627, Czech Republic

***Abstract*— In this paper, we present and experimentally evaluate a real-time 10 Gbps free-space optical (FSO) link under varying atmospheric conditions. In bandwidth-craving wireless technologies due to the ubiquitous consumption by internet of things devices and requiring high data rate online services, unlicensed FSO systems can be a promising candidate to satisfy the network capacity of the existing data communications technologies. In this work, we verify the experiment using small form-factor pluggable transceivers mounted FPGA as a FSO transmitter and receiver. Here, a high-speed single FSO link is proposed and its performance under turbulence and fog conditions using the dedicated indoor atmospheric chamber is evaluated. We show that the proposed system under the turbulence condition with a scintillation index of 0.35 offers the same data rate as the link under a clear channel, while the bit error rate increases from 10^{-12} to 5×10^{-4}.**

***Keywords*— FSO, Fog, Turbulence, Last Mile Access**

I. Introduction

As a branch of optical wireless communications (OWC), free-space optics (FSO) has become increasingly attractive to numerous applications in several environments [1, 2]. This has been driven by the ability to compensate for the required bandwidth that radio frequency (RF) based wireless communications systems are unable to provide as well as the ease, and time of installation that optical fiber (OF) communications cannot achieve. Due to its massive license-free spectrum (up to ≅ 400 THz), high data rates in the order of terabits/second, backbone network capability, inherent security at the physical layer, and insignificant inter-channel interference, FSO stands as the preeminent candidate to unlock the mobile spectrum congestion (bandwidth bottleneck) issue, which has been predicted to increase a thousand-fold over the next decade [3]. While 2-10% of the global power consumption is responsible by the data communication technologies, energy-efficient FSO systems are also known for potentially being economically green compared to RF [3]. In the race for reaching high data flow (> Gbps) over short distances, also known as 'last mile' or 'last kilometer' access, optical communications present significant advantages when compared with the radio even in the millimeter-wave (mmW) band [3]. High performance of data propagation and highly directional FSO communications systems can be deployed as part of back and front haul traffic in areas where cable-based fixed links are not economical [4]. One of the promising economic reasons for this is the availability of components, which are also extensively used in the matured OF communications technology. In the deployment of future wireless networks (i.e., fifth generation (5G) and beyond), FSO (both visible and infrared bands) have an important role in addressing the growing security threat due to its increase in types of services and devices used in broadband access. Furthermore, FSO can be easily implemented, particularly for the last mile access networks, where high data rates communications over a few kilometers of transmission link span are required [3].

Recently, commercially available technologies of mmW and Terragraph by Facebook offer up to 1 Gbps throughput over a range of 150 m [5]. However, the commercial FSO systems can provide much higher data rates of ≤10 Gbps over a link span of up to 1.5 km [3, 5]. FSO systems employing advanced modulation and multiplexing schemes, potentially achieving up to hundreds of Tbps employing orbital angular momentum, wave division multiplexing, mode division multiplexing, and space division multiplexing have been reported in [6, 7] and [8]. However, most of the systems are costly and complex with off-line measurements and analysis. In this paper, we present a real-time 10 Gbps FSO system implementation based on small form-factor pluggable (SFP) mounted xilinx field programmable gate arrays (FPGA), which can be used in both last meter/last mile access, and presents a potential replacement of mmW technology, that can promptly be integrated to the backbone OF networks as in Terragraph. The proposed system is cost effective, robust, and easily assembled. We evaluate the performance of the system under various atmospheric conditions using a dedicated indoor atmospheric chamber

The paper is organized as follows: Section 2 describes the FSO system and provides all of the design considerations. Section 3 presents the results and discussion of the measured data. Finally, Section 4 concludes the paper.

II. System design

The schematic block diagram of the experimental setup is presented in Fig. 1. The transmitter (Tx) unit consists of Zynq ultrascale+ FPGA for generating a 10 Gbps optical link at 1550 nm through a gigabit transceiver (GTH) port wired to a SFP+

2×2 quad-module connector. An erbium doped fiber amplifier (EDFA) is used to amplify the optical signal before being transmitted across the free space channel using a single mode fiber (SMF) integrated kinematic collimator mounting adaptor. Note that, the kinematic adaptor provides pitch and yaw adjustment, thus allowing the collimated beam to be easily steered while aligning the system.

The propagated signal is coupled into multimode fiber (MMF) with a core size of 105 µm using a condenser/convex lens with the effective focal length (EFL) of 44 mm. The output of the MMF is injected into the SFP module connector mounted on the FPGA board to make a real-time bit by bit comparison to estimate the received bits and, therefore the BER. Extracted information of the link from the FPGA connected to the PC is displayed in Vivado® Xilinx using the customizable LogiCORE™ IP Integrated bit error rate tester (IBERT) core for UltraScale+ architecture GTH transceivers. UltraScale™ GTH transceivers offer up to 16.3 Gbps with a maximum optical transmit power and receiver (Rx) sensitivity of 4 dBm and >-16 dBm, respectively [9]. While the typical plug and play 10GBASE SFPs provide the same transmit and receive power levels with the data rate of 10.312 Gbps [10]. The maximum link margin loss of the proposed FSO link is up to ~20 dB, which is dominated by the loss due to misalignment and optics in our case. The green laser is used to estimate the fog attenuation experienced by the system and on off keying (OOK) modulated red laser is used to estimate the scintillation index. The temperature gradient measurement is done by 17 distributed temperature sensors as shown in Fig. 1.

In the context of optical communications, the received signal is given as:

$$y(t) = h(t) * x(t) + n(t), \tag{1}$$

where x is the transmitted signal, n is additive white Gaussian noise (AWGN) with variance σ_n^2, * is the convolution symbol and h is the channel gain, which is given by:

$$h = h_a h_t, \tag{2}$$

where h_a and h_t are the attenuation constants due to the atmospheric channel and turbulence, respectively. For an FSO link, h_a is given by Beer's law as [11]:

$$h_a = e^{-\gamma l}, \tag{3}$$

where l is the link length in m and γ is the attenuation coefficient in m^{-1}. The attenuation coefficient γ models the atmosphere and is the combination of absorption and scattering coefficients expressed as a function of wavelength. γ is given by [11]:

$$\gamma(\lambda) = \alpha_m(\lambda) + \alpha_a(\lambda) + \beta_m(\lambda) + \beta_a(\lambda), \tag{4}$$

where, $\alpha_m(\lambda)$ and $\alpha_a(\lambda)$ are the molecular and aerosol absorption coefficients, respectively, and $\beta_m(\lambda)$ and $\beta_a(\lambda)$ are the molecular and aerosol scattering coefficients, respectively. The transmission wavelength in FSO is selected such that, it coincides with the atmospheric transmission window [12] hence, scattering governs the atmospheric attenuation coefficient and as a result $\gamma(\lambda) \approx \beta_a(\lambda)$. $\beta_a(\lambda)$, which is expressed as [13]:

$$\beta_a(\lambda) = \frac{3.91}{V}\left(\frac{\lambda}{550\text{ nm}}\right)^{-q}, \tag{5}$$

where, V is the meteorological visibility in km and q is the size distribution of scattering particles, for which Kruse model is considered in this paper, as given by [14]:

$$q = \begin{cases} 1.6 & V > 50\text{ km} \\ 1.3 & 6\text{ km} < V < 50\text{ km} \\ 0.16V + 0.34 & 1\text{ km} < V < 6\text{ km} \\ V - 0.5 & 1\text{ km} < V < 1\text{ km} \\ 0 & V < 0.5\text{ km} \end{cases}, \tag{6}$$

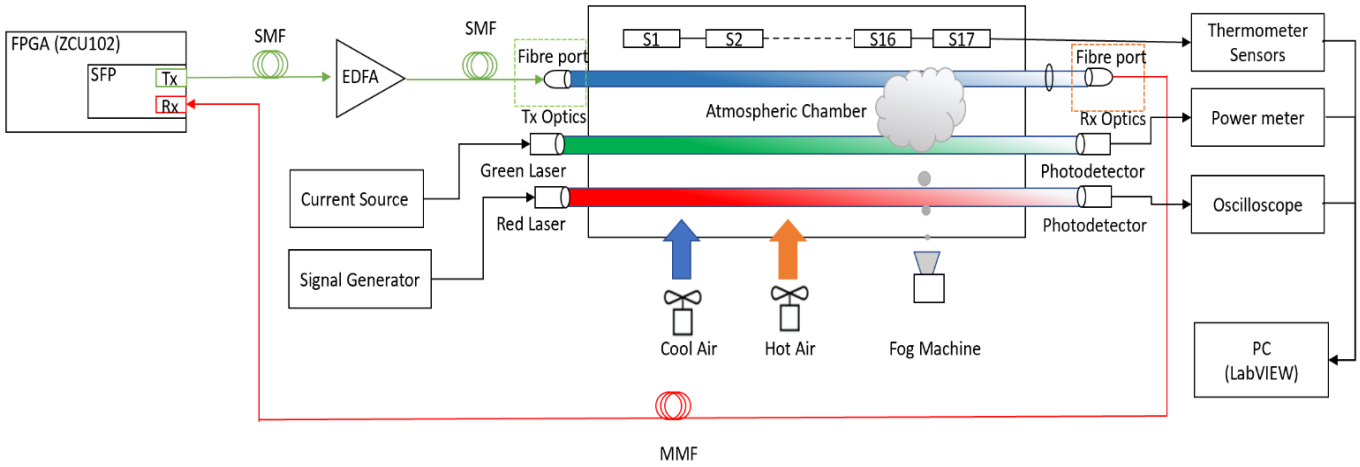

Fig. 1. Experimental setup.

The optical intensity I of a wave propagating in a turbulence channel undergoes a random fading effect with the normalized variance or the scintillation index, which is given as [15]:

$$\sigma_I^2 = \frac{\langle I^2 \rangle - \langle I \rangle^2}{\langle I \rangle^2}, \tag{7}$$

where $\langle . \rangle$ denotes the ensemble average equivalent to long-time averaging with the assumption of an ergodic process. Assuming plane wave propagation, σ_I^2 is given by [16]:

$$\sigma_I^2(D) = \exp\left[\frac{0.49\,\sigma_R^2}{\left(1 + 0.653d^2 + 1.11\sigma_R^{\frac{12}{5}}\right)^{\frac{7}{6}}} + \frac{0.51\,\sigma_R^2\left(1 + 0.69\,\sigma_R^{\frac{12}{5}}\right)^{-\frac{5}{6}}}{(1 + 0.9d^2 + 0.621\,d^2\sigma_R^2)^{\frac{12}{5}}}\right] - 1, \tag{8}$$

where $d = \frac{D}{2}\sqrt{\frac{k}{l}}$ is the circular aperture scaled by Fresnel zone provided, k is the wavenumber and D is the Rx aperture diameter. σ_R^2 is Rytov variance showing the strength of the turbulence is expressed by:

$$\sigma_R^2 = 1.23C_n^2k^{7/6}l^{11/6}, \tag{9}$$

The strength of turbulence can be classified as weak ($\sigma_R^2 < 1$), moderate ($\sigma_R^2 \cong 1$) and strong ($\sigma_R^2 > 1$) [17]. For weak to moderate we can assume that $\sigma_I^2 = \sigma_R^2$. C_n^2 is the refractive index structure parameter and is expressed as [18]:

$$C_n^2 = \left[79 \times 10^{-6}\frac{P}{T^2}\right]C_T^2, \tag{10}$$

where, P is the atmospheric pressure in mbar, T is temperature in kelvin and C_T is the temperature structure parameter, which is given by [18]:

$$C_T = \sqrt{\langle \delta T^2 \rangle r^{-1/3}}, \tag{11}$$

where δT refers to the temperature differential between two points separated by a distance r. For weak turbulence, the turbulence induced fading gain is given as [19]:

$$h_t = e^{\chi + iS}, \tag{12}$$

where S is the phase and χ is the fading log-amplitude having normal distribution with mean μ and variance σ_χ^2. The signal to noise ratio at the Rx for OOK is expressed as [20]:

$$\text{SNR} = \frac{(RP_{\text{rx}})^2}{\sigma_n^2}, \tag{13}$$

where R is the responsivity of the Rx in A/W and σ_n^2 is the combination of shot noise and thermal noise modelled as AWGN variance. The received power can be expressed as a function of the transmit power and the system losses, which is given by:

$$P_{\text{rx}} = 10^{\frac{(L_{\text{Geo}})}{10}} \times 10^{\frac{(L_{\text{Atm}})\frac{l}{1000}}{10}} \times 10^{\left(\frac{L_{\text{Misc}}}{10}\right)}P_{\text{tx}}, \tag{14}$$

where P_{tx} is the transmitted power, L_{Geo} is the geometrical loss, L_{Atm} is the atmospheric loss and L_{Misc} is the miscellaneous loss including coupling losses due to optics to

Table 1. Parameters and Specification of the system.

	Parameter	Specification
Transmitter	Tx power (P_{tx})	5 dBm
	Tx optics (Threaded Kinematic adapter)	D_{tx}: 6.5 mm
	SFP+ Tx power	4 dBm
	Tx beam divergence (θ)	0.279 mrad
Receiver	FPGA, SFP+ modules (2×2 quad-connector) - ZCU102 (Ultrascale +) evaluation kit	Throughput: 10.3125Gbps Clock frequency: 156.2 MHz
	Rx power	-6 dBm
	Rx optics - Lens	Effective focal length: 44 mm D_{rx}: 50 mm
	SFP+ sensitivity	-16 dBm
Other parameters	SFP+ wavelength	1550 nm
	Tx core diameter (SMF)	8.2 μm
	Rx core diameter (MMF)	105 µm

fiber and optics coupling. Geometric loss occurs due to the spreading of the transmitted beam, increasing to a size larger than the Rx aperture D_{rx}. The geometric loss in dB is given by [21]:

$$L_{\mathrm{Geo}}(\mathrm{dB}) = 20\log_{10}\left(\frac{D_{\mathrm{rx}}}{D_{\mathrm{tx}} + l \times \theta}\right), \quad (15)$$

where D_{tx}, D_{rx} are the Tx and the Rx aperture diameters in meters, respectively and θ is the Tx beam divergence. L_{Atm} is the atmospheric attenuation in dB/km and is given by [20]:

$$L_{\mathrm{Atm}}\left(\frac{\mathrm{dB}}{\mathrm{km}}\right) = 4.343\beta_a(\lambda). \quad (16)$$

III. Results and Discussions

We have experimentally investigated the 10 Gbps FSO link shown in Fig. 2. Fig. 2(a) pictures a foggy chamber and temperature sensors. Fog is generated using the fog machine and the turbulence regime is created using hot and cool fans injected into the chamber. The temperature gradient measurement within the atmospheric chamber was taken by using 17 distributed temperature sensors S1 to S17 with a spacing of ~25 cm each along the chamber. Utilization of temperature sensors is to estimate the channel refractive index structure coefficient, C_n^2 within the chamber by following (10). The alignment and performance analysis of the 10 Gbps link is carried out in 7.2-meter atmospheric chamber. Fig. 2(b) depicts the Tx unit consisting of a signal generator coupled to a red laser (685 nm). Both red and green lasers are powered independently. A 10 Gbps non-return to zero on/off keying (NRZ-OOK) signal format is generated via the FPGA and an EDFA is used to amplify the optical signal power before being transmitting through the SMF cable, see Fig. 2(c). At the Rx side, MMF has been used to couple the signal into the SFP transceiver module. Additionally, two photodetectors (PD) were used at the end of the chamber to capture a red laser and a green laser. A red laser beam is transmitted through the chamber and after detection captured by sampling oscilloscope to estimate the turbulence effect on channel in terms of scintillation index σ_I^2.

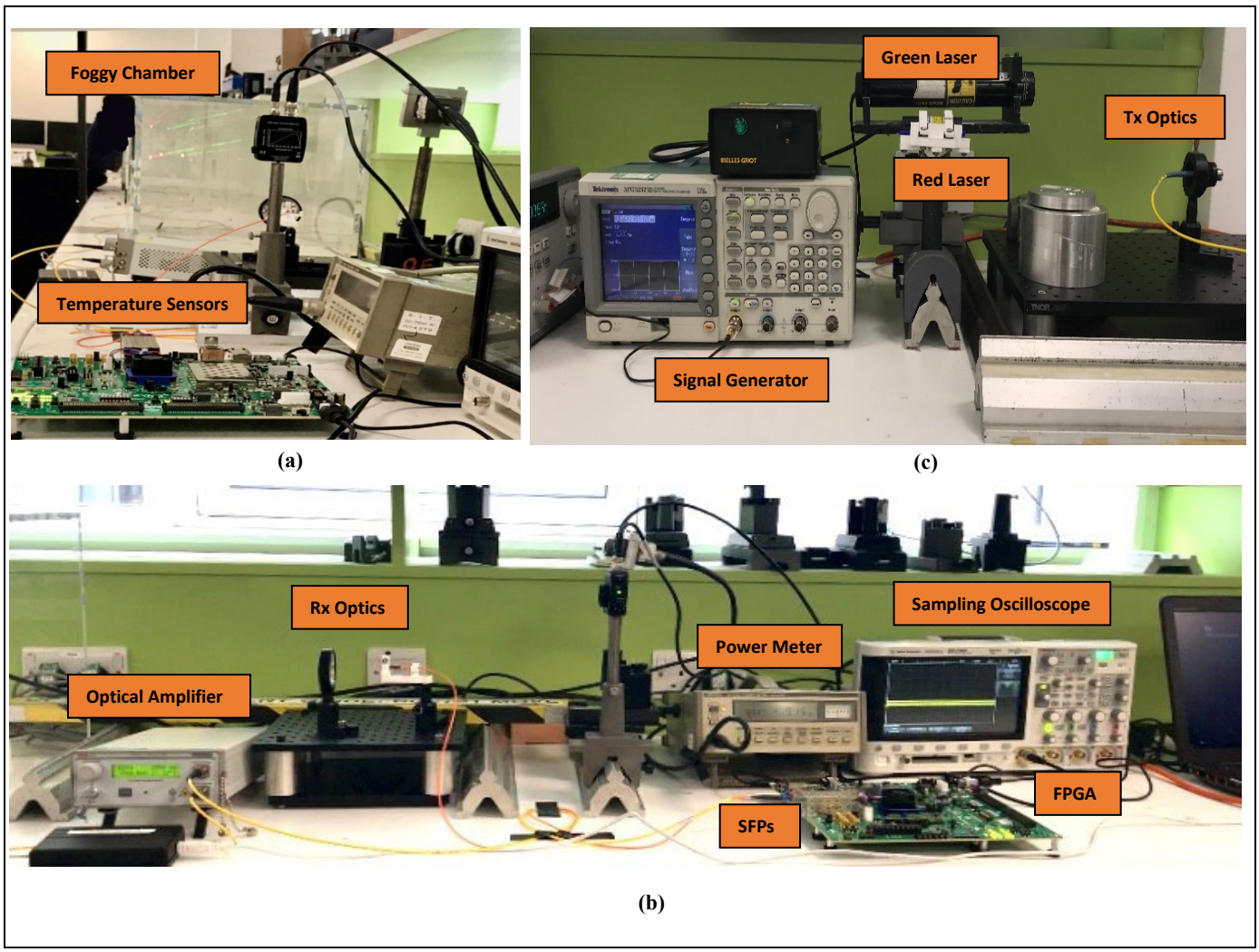

Fig. 2 (a) Channel setup when fog is injected, and (b) Rx setup with power meter connected to the green laser photodetector to estimate visibility and sampling oscilloscope connected to measure scintillation index through red laser photodetector. Oscilloscope, power meter, and temperature sensors are connected to PC to read the measurements via LabVIEW. SFP transceiver mounted FPGA is connected to PC. (c) Tx setup with green and red laser to estimate the atmospheric and turbulent condition in the chamber.

The green laser and a photodetector connected to the power meter is then utilized to calculate the visibility (V) of the chamber is determined by following the method outlined in [19] and (5) under foggy conditions within the chamber. The channel condition and parameters are analysed using Vivado, which provides important characteristics of the link such as BER, number of errors, the data rate, and link stability. We observed the clear channel and the link parameters for approximately 90 seconds while an average of 3.8×10^{13} bits were transmitted within this period. While observing the system we carried out the BER measurement of the link, which was 2.6×10^{-12} and the maximum throughput of 10.312 Gbps. Subsequently, we performed the measurements under different conditions of fog and turbulence. Considering the clear channel $V > 20$ km, a light fog regime was generated within the chamber to increase the attenuation of the link to ~0.2 dB, thus resulting in increased BER to 5×10^{-5}. We reduced V further to ~8.5 m while the attenuation was increased to 13 dB with the BER of 1.9×10^{-4}.

In the next experiment, we tested turbulence within the chamber by injecting cool and hot air using two fans and two heaters. With weak turbulence of 0.35 of σ_I^2, the availability of the link and data rate remains intact, however, BER increased. In consideration of the realistic link length for last mile access and short/mid-range distance, we have made further analysis of the link spans of 50, 160, and 200 m. With the observation in

Table 2: Parameters and specification of the system. C_n^2 and σ_I^2 denotes the refractive index structure coefficient and the scintillation index, respectively.

Link Span	Parameter	Value	BER
l = 7.2 m (Experimental)	Visibility (clear) Attenuation	20 km 0 dB	2.6×10^{-12}
	Visibility Attenuation	385 m 0.2 dB	5×10^{-5}
	C_n^2 σ_I^2	$6.8 \times 10^{-11} \mathrm{m}^{\frac{-2}{3}}$ 0.16	1.5×10^{-5}
	Visibility Attenuation	~8.5 m 13 dB	1.9×10^{-4}
	C_n^2 σ_I^2	$1.45 \times 10^{-10} \mathrm{m}^{\frac{-2}{3}}$ 0.35	5×10^{-4}
l = 50 m (Simulation)	Visibility Attenuation	4.2 km 0.2 dB	5×10^{-5}
	C_n^2 σ_I^2	$1.95 \times 10^{-12} \mathrm{m}^{\frac{-2}{3}}$ 0.16	1.5×10^{-5}
	Visibility Attenuation	65 m 13 dB	1.9×10^{-4}
	C_n^2 σ_I^2	$4.27 \times 10^{-12} \mathrm{m}^{\frac{-2}{3}}$ 0.35	5×10^{-4}
l = 160 m (Simulation)	Visibility Attenuation	13.5 km 0.2 dB	4.9×10^{-5}
	C_n^2 σ_I^2	$2.31 \times 10^{-13} \mathrm{m}^{\frac{-2}{3}}$ 0.16	6.6×10^{-4}
	Visibility Attenuation	208 m 13 dB	≈ 1 (0.24)
	C_n^2 σ_I^2	$5.06 \times 10^{-13} \mathrm{m}^{\frac{-2}{3}}$ 0.35	5.2×10^{-3}
l = 200 m (Simulation)	Visibility Attenuation	16.9 km 0.2 dB	6.1×10^{-3}
	C_n^2 σ_I^2	$1.54 \times 10^{-13} \mathrm{m}^{\frac{-2}{3}}$ 0.16	6.7×10^{-3}
	Visibility Attenuation	261 m 13 dB	≈ 0.5 (0.32)
	C_n^2 σ_I^2	$3.36 \times 10^{-13} \mathrm{m}^{\frac{-2}{3}}$ 0.35	2.1×10^{-2}

accordance with V, σ_I^2 and C_n^2, we considered similarly the attenuated channel with 0.2 and 13 dB as the reference and calculated V. For the turbulence channel, assuming that the scintillation index (i.e., the intensity of turbulence) in both links under weak and moderate turbulence regimes are 0.16 and 0.35, respectively, we determined C_n^2 for the links.

Table 2 describes the channel under the different controlled atmospheric experimental conditions and the parameters of the channel impairments. Even though, the attenuation of the clear channel is 0 dB, note that the additional losses due to the Tx and the Rx optics and misalignment are kept to the minimum level. During the experiment, we observed a number of sources, which contributed additional losses including (*i*) coupling free space optical source into the optical fibre at the Rx unit; and (*ii*) light coupling from SFP to SMF (Tx) and MMF to the PD at the Rx. Note, SFP requires the use of an attenuator to stabilize the optical power and to make a connection with the module. In this work, we used a 105 μm core size MMF at the Rx, see Table 1, which is disadvantageous in the turbulent channel as the smaller the core size the higher the loss due to beam wandering misalignment [17]. In the experimental setup (i.e., a length of 7.2 m) and up to 150 m links, the beam spot size compared with the Rx aperture is small. Therefore, the geometrical loss L_{Geo} is not considered. In addition, we assumed that the BER for the FSO link for up to 150 m is the same as the 7.2 m link span as described in Table 2. For the 7.2 m link span, the Tx power P_{tx} and Rx power P_{rx} are 5 and -6 dBm, respectively, thus resulting in the total loss (i.e., coupling, misalignment, and optics) of 11 dB. For the 160 m link, L_{Geo} is introduced and L_{Geo} is increased accordingly with the link span, see Table 2. With the introduction of fog with 13 dB of attenuation, both 160 and 200 m links are intolerable. This is due to the additional L_{Geo} values of 0.2 and 1.9 dB for the 160 and 200 m links, respectively, which exceeds the system margin. The link unavailability is attributable to the aperture of the Rx diameter D_{rx} size being smaller than the Tx beams footprint, which increases with distance, thus wasted "overfill" energy. Therefore, the coupling fibre core size and larger D_{rx} or smaller beam transmitted divergence (collimated) according to the turbulence intensity and link distance are suggested to be considered to reduce this additional loss. Increasing P_{tx}will also ease the attenuation due to the fog over a longer link span. Considering that, the misalignment loss is negligible, P_{rx} for 160 and 200 m is 4.8 and 3.1 dBm, respectively under clear channel with geometrical loss. With the misalignment loss included in the system, P_{rx}will then change on -6.2 and -7.9 dBm, respectively.

IV. CONCLUSION

In this work, we demonstrated an experimental real-time FPGA implementation of a 10 Gbps FSO link and investigated its performance under different atmospheric conditions. We made the bit by bit comparison using customizable LogiCORE™ IP IBERT core for UltraScale+ architecture GTH transceivers. We discussed the causes incurring additional loss of the system which can be addressed by using different or larger Rx aperture and smaller collimated Tx beam divergence. Additionally, we considered 50, 160, and 200 m link spans under the same atmospheric conditions and investigated the link performances. We showed that the proposed FSO link can be improved by reducing misalignment and geometrical losses. We outlined that, the proposed FSO link under heavy fog condition offers the same data rate but of course increased BER (i.e., increasing from 10^{-12} to 10^{-4}) over a 7.2 m link range. Under weak turbulence, we observed that the link BER is increased from 10^{-12} to 10^{-4} due to both phase and amplitude variations.

ACKNOWLEDGMENT

This project is supported by intensive industrial innovation program northeast, United Kingdom (IIIP NE) - 25R17P01847 and is partly funded by the European regional development fund (ERDF).

REFERENCES

[1] M. Uysal, C. Capsoni, Z. Ghassemlooy, A. Boucouvalas, and E. Udvary, *Optical Wireless Communications : An Emerging Technology* (Signals and Communication Technology). Springer International Publishing, 2016.

[2] Z. Ghassemlooy, S. Rajbhandari, and W. Popoola, *Optical wireless communications: system and channel modelling with MATLAB*. CRC Press; 2 edition (8 April 2019), 2018.

[3] A. K. Majumdar, Z. Ghassemlooy, and A. A. B. Raj, "Principles and applications of free space optical communications," (in English), 2019. [Online]. Available: https://digital-library.theiet.org/content/books/te/pbte078e.

[4] Y. Alfadhli *et al.*, "Real-Time FPGA Demonstration of Hybrid Bi-Directional MMW and FSO Fronthaul Architecture," in *2019 Optical Fiber Communications Conference and Exhibition (OFC)*, 3-7 March 2019 2019, pp. 1-3.

[5] "terragraph | Solving The Urban Bandwidth Challenge." https://terragraph.com/ (accessed 15-July-2020).

[6] E. Ciaramella *et al.*, "1.28 terabit/s (32x40 Gbit/s) wdm transmission system for free space optical communications," *IEEE Journal on Selected Areas in Communications,* vol. 27, no. 9, pp. 1639-1645, 2009, doi: 10.1109/JSAC.2009.091213.

[7] Y. Ren *et al.*, "Atmospheric turbulence effects on the performance of a free space optical link employing orbital angular momentum multiplexing," *Opt. Lett.,* vol. 38, no. 20, pp. 4062-4065, 2013/10/15 2013, doi: 10.1364/OL.38.004062.

[8] M. M. Abadi, M. A. Cox, R. E. Alsaigh, S. Viola, A. Forbes, and M. P. J. Lavery, "A space division multiplexed free-space-optical communication system that can auto-locate and fully self align with a remote transceiver," *Scientific Reports,* vol. 9, no. 1, p. 19687, 2019/12/23 2019, doi: 10.1038/s41598-019-55670-1.

[9] "UltraScale and UltraScale+ GTH Transceivers." https://www.xilinx.com/support/documentation-navigation/design-hubs/dh0086-ultrascale-gth-tabbed-hub.html (accessed 15-July-2020).

[10] "10G SFP+ " https://www.fs.com/c/10g-sfp-plus-63 (accessed 15-July-2020).

[11] E. Leitgeb, S. S. Muhammad, C. Chlestil, M. Gebhart, and U. Birnbacher, "Reliability of FSO links in next generation optical networks," in *Proceedings of 2005 7th International Conference Transparent Optical Networks, 2005.*, 7-7 July 2005 2005, vol. 1, pp. 394-401 Vol. 1, doi: 10.1109/ICTON.2005.1505829.

[12] W. O. Popoola, "Subcarrier intensity modulated free-space optical communication systems,", PhD Thesis, Northumbria University, UK, 2009.

[13] M. K. El-Nayal, M. M. Aly, H. A. Fayed, and R. A. AbdelRassoul, "Adaptive free space optic system based on visibility detector to overcome atmospheric attenuation," *Results in Physics,* vol. 14, p. 102392, 2019/09/01/ 2019, doi: https://doi.org/10.1016/j.rinp.2019.102392.

[14] L. D. M. P. W. Kruse, and R. B. McQuistan, *Elements of Infrared Technology: Generation, Transmission, and Detection* 1963.

[15] S. Rajbhandari, Z. Ghassemlooy, P. A. Haigh, T. Kanesan, and X. Tang, "Experimental Error Performance of Modulation Schemes Under a Controlled Laboratory Turbulence FSO Channel," *Journal of Lightwave Technology,* vol. 33, no. 1, pp. 244-250, 2015, doi: 10.1109/JLT.2014.2377155.

[16] M. A. Khalighi, N. Aitamer, N. Schwartz, and S. Bourennane, "Turbulence mitigation by aperture averaging in wireless optical systems," in *2009 10th International Conference on Telecommunications*, 8-10 June 2009 2009, pp. 59-66.

[17] M. M. Abadi, Z. Ghassemlooy, N. Mohan, S. Zvanovec, M. R. Bhatnagar, and R. Hudson, "Implementation and Evaluation of a Gigabit Ethernet FSO Link for 'The Last Metre and Last Mile Access Network'," in *2019 IEEE International Conference on Communications Workshops (ICC Workshops)*, 20-24 May 2019, pp. 1-6, doi: 10.1109/ICCW.2019.8757150.

[18] H. Kaushal *et al.*, "Experimental Study on Beam Wander Under Varying Atmospheric Turbulence Conditions," *IEEE Photonics Technology Letters,* vol. 23, no. 22, pp. 1691-1693, 2011, doi: 10.1109/LPT.2011.2166113.

[19] M. Ijaz, Z. Ghassemlooy, J. Pesek, O. Fiser, H. L. Minh, and E. Bentley, "Modeling of Fog and Smoke Attenuation in Free Space Optical Communications Link Under Controlled Laboratory Conditions," *Journal of Lightwave Technology,* vol. 31, no. 11, pp. 1720-1726, 2013, doi: 10.1109/JLT.2013.2257683.

[20] R. Paudel, Z. Ghassemlooy, H. Le-Minh, and S. Rajbhandari, "Modelling of free space optical link for ground-to-train communications using a Gaussian source," *IET Optoelectronics,* vol. 7, no. 1, pp. 1-8, 2013, doi: 10.1049/iet-opt.2012.0047.

[21] E. K. S. Bloom, J. Schuster, and H. Willebrand, "Understanding the performance of free-space optics [Invited]," *J. Opt. Netw. 2,* pp. 178-200, 2003.